Nonlinear Dynamics of Bloch Wave Packets in Honeycomb Lattices

Mark J. Ablowitz and Yi Zhu

Abstract Nonlinear waves in deformed optical honeycomb lattices are investigated. Discrete couple mode equations are used to find higher order continuous nonlinear Dirac systems which are employed to describe key underlying phenomena. For weak deformation and nonlinearity the wave propagation is circular–ellliptical. At strong nonlinearity the diffraction pattern becomes triangular in structure which is traced to appropriate nonequal energy propagation in momentum space. At suitably large deformation the dispersion structure can have nearby Dirac points or small gaps. The effective dynamics of the wave packets is described by two maximally balanced nonlocal nonlinear Schrödinger type equations.

1 Introduction

Wave propagation in honeycomb lattices has attracted considerable interest in physics and applied mathematics. One of the main reasons to understand these lattices and their behavior is due to the recent fabrication of the new material graphene and its success in numerous applications [1]. Many of the important properties associated with graphene come from the two-dimensional honeycomb

M. J. Ablowitz
Department of Applied Mathematics, University of Colorado, 526 UCB,
Boulder, CO 80309-0526, USA

Y. Zhu (✉)
Zhou Pei-Yuan Center for Applied Mathematics, Tsinghua University,
Beijing 100084, China
e-mail: yizhu@tsinghua.edu.cn

Progress Optical Sci., Photonics (2013): 1–26
DOI: 10.1007/10091_2012_27

Published Online: 30 January 2013

arrangement of its atoms which has major effect on how the associated matter waves propagate. More specifically, the spectrum of the Schrödinger operator with a honeycomb lattice exhibits conical structure in the neighborhood where two dispersion branches touch; these locations are referred as Dirac points. In the vicinity of the Dirac points, the dispersion relation locally forms a double-cone, referred as a Dirac cone. This special geometric structure gives rise to two independent Bloch wave envelopes or packets. In other words the conical dispersion relation admits the propagation of massless Fermions. Interestingly important and novel phenomena are related to these unusual electronic excitations; e.g., anomalous integer quantum Hall effect, Klein tunneling, enhanced conductivity etc. [1–3]. Other fields where honeycomb lattices play important roles include electromagnetic waves propagating in photonic crystals with a honeycomb background [4] and ultra cold atoms trapped in optic induced honeycomb lattices [5, 6].

On the other hand even though electromagnetic waves which are classical waves obey Maxwell equations, the propagation of light in a paraxial photonic crystal can be described by a lattice nonlinear Schrödinger (NLS) Eq. (1), see for example, [7]. In order to stablize the lattice, for instance, in optically induced crystals, the lattice intensity is often much higher than the intensities of the propagation waves [8–10]. This setup leads to the strong potential or so-called tight-binding limit. In this context, coupled-mode theory provides an approximate model for the wave packets which are represented as discrete evolution equations [11]. In the case when the simple background lattice is square or rectangular the governing Bloch envelope equation can often be reduced to a discrete nonlinear Schrödinger equation; this generally corresponds to single band approximations [12, 13]. But when the background lattice is not simple, such as a honeycomb-hexagonal lattice, one finds that the fundamental governing Bloch envelope equation satisfies a discrete nonlinear Dirac system which describes the wave dynamics associated with the Dirac cone [14–16]. From a mathematical point of view these problems have certain common features; in particular wave envelopes associated with Bloch modes and the associated nonlinearity are centrally important in the analytical description.

The study of the interplay between periodicity and nonlinearity leads to important mathematical questions. Periodicity relates to the band structure of the dispersion relation and Bloch waves which are similar in spirit to plane waves in Fourier analysis. In many cases the nonlinearity induces pure self phase modulation. But nonlinearity can also couple waves between different Fourier modes or Bloch bands. In simple lattices Bloch envelopes can lead to interesting localized structures which propagate in the gap regimes of the spectrum; they are sometimes referred to as gap solitons. Associated with such gaps in the spectrum many different types of propagating localized waves have been found; examples include but are not limited to dipole solitons, vortex solitons and soliton trains [8–10, 17–23]. As in the simple lattice case honeycomb lattices can also admit gap solitons [4, 12]. These solitons are often considered theoretically as bifurcations from the Bloch-band edges into the band gaps [24–26]. Similarly solitons can sometimes be found in near periodic and complex media cases [27–29].

Wave propagation in honeycomb lattices when the potential is strong (the tight-binding limit) was first considered by Wallace in 1947 [30]; this work paved the way for researchers to begin to understand the theoretical underpinnings of the linear wave propagation in honeycomb lattices. The first experimental fabrication of the material graphene was carried out by Geim and Novoselov [1, 2]. Inspired by the success of graphene, honeycomb structures have been studied in many fields. In optics, gap solitons were studied in honeycomb lattices [4, 12] and conical diffraction in honeycomb lattice was observed in [4, 31]. They experimentally demonstrated conical diffraction and gap solitons in honeycomb lattices. Theoretically speaking, wave dynamics associated with the Dirac points in honeycomb lattices has recently been considered. Ablowitz and Zhu found a general discrete envelope Dirac wave system in the tight-binding limit and studied the associated nonlinear dynamics, including conical and triangular diffraction of the optical wave field [14, 15, 32]. In the context of Bose-Einstein condensation, Haddad and Carr studied nonlinear atomic waves propagating in honeycomb optical lattices [16] in the tight binding limit. Haldane and Raghu studied linear propagation of electromagnetic waves in the full Maxwell equations [33, 34]; Ablowitz and Zhu analyzed the wave propagation in the shallow potential and weak nonlinear limits [35]. Wave dynamics in $\mathcal{PT}$-symmetric honeycomb lattices were studied in [36, 37] and symmetry breaking and wave dynamics in deformed honeycomb lattices were studied in [31, 32, 38, 39]. Fefferman and Weinstein rigorously proved the existence of Dirac points for a perfect honeycomb lattice in a generic regime and obtained the first order approximation in the neighborhood of Dirac cones [40].

As indicated above, one of the key features of honeycomb lattices is the existence of the Dirac cones and the associated envelope wave dynamics. This paper addresses the novel aspects of the nonlinear propagation of wave packets near the Dirac cone in two-dimensional (2-D) honeycomb lattices. The outline of this paper is as follows. In Sects. 2–3 the fundamentals of periodic optical and honeycomb lattices are discussed. In Sect. 4 the discrete nonlinear Dirac system is derived; we include a deformation parameter ρ. Depending on the size of ρ in Sect. 5 we explain that one might or might not have Dirac points. The continuum limit of the discrete system associated with the special points is studied in Sect. 6; here we obtain the nonlinear Dirac equation and discuss the associated conical dynamics. In Sect. 7 we show the symmetry breaking of the conical dynamics due to the nonlinearity which also requires the higher order dispersive terms to describe the dynamics. We then study deformed honeycomb lattices in Sect. 8. The effect of nonlinearity on the wave propagation in the various deformation regions is explored in the remaining parts of the paper. Novel nonlinear wave equations are derived in the two different regimes: (i) where there are two neighboring Dirac points (ii) no Dirac points. We find asymptotically valid equations to be nonlocal NLS equations which we refer to as NLS Kadomtsev–Petviashvili (KP) type equations—or NLSKP type equations; i.e., they are analogs of nonlocal KP equations which arise in water waves [41].

2 2-D Optical Periodic Lattices

As mentioned earlier, electromagnetic waves propagating in an inhomogeneous Kerr nonlinear medium can often be described by a two-dimensional nonlinear Schrödinger Eq. (7); this equation written in dimensionless form is given by

$$i\psi_z + \nabla^2\psi - \delta V(\mathbf{r})\psi + \sigma|\psi|^2\psi = 0. \tag{1}$$

Here $\mathbf{r} = (r_1, r_2)$ is the transverse coordinate; z is the propagation direction; the potential, $V(\mathbf{r})$ is a real periodic function which represents the transverse variation of the refractive index, and δ represents its order of magnitude; σ is the nonlinear coefficient which is positive for focusing nonlinearity and negative for defocusing nonlinearity. In Bose–Einstein condensation this equation is usually called the Gross–Pitaevskii (GP) equation. In this context it describes the wave propagation associated with the ultra cold atoms trapped in a periodic lattice [5].

The geometric distribution of local minima of the potentials, also called sites, determines the main features of the periodic potential. These sites are the positions of the potential wells. In optics, they have increased refractive index the electromagnetic field is attracted to the sites. A 2-D periodic function has two periods along two different directions which we call primitive lattice vectors. Let $\Gamma \simeq \mathbb{Z}^2$ denote a two-dimensional lattice generated through the basis $\{\mathbf{v}_1, \mathbf{v}_2\}$, i.e.,

$$\Gamma = \{m\mathbf{v}_1 + n\mathbf{v}_2 : \quad m, n \in \mathbb{Z}\}.$$

The primitive unit cell Ω is defined as

$$\Omega = \{q_1\mathbf{v}_1 + q_2\mathbf{v}_2 : q_j \in [0, 1)\}.$$

The primitive cell Ω is the fundamental tile of a tessellation of the plane associated with the lattice Γ, i.e., $\mathbb{R}^2 = \bigcup_{\mathbf{v}\in\Gamma}(\Omega + \mathbf{v})$.

For simple 2-D lattices, there is only one site (local minimum) per cell. All sites can be generated by a starting point with two discrete translational symmetries, i.e., two periods $\mathbf{v}_1$ and $\mathbf{v}_2$. Interactions between two sites are the same as the interactions between two cells. Typical examples are square lattices and triangular lattices. In so-called non-simple lattices, there are multiple sites per cell. In addition to periodicity, extra freedoms are needed to identify the distributions of the sites. They are the inner freedoms which, for instance, describe the distances between sites in the same cell or depths of the sites. All sites are identical under translational symmetries in simple lattices while non-simple lattices contain at least two different types of sites. A honeycomb lattice is such a structure. It has two sites per cell. The inner parameters (distance between two sites and depths of each site) play very important roles. The dual lattice Γ' is spanned by the dual basis vectors $\mathbf{k}_1$ and $\mathbf{k}_2$ where $\mathbf{k}_m \cdot \mathbf{v}_n = 2\pi\delta_{mn}$. Namely $\Gamma' = \{m\mathbf{k}_1 + n\mathbf{k}_2 : \quad m, n \in \mathbb{Z}\}$.The primitive dual unit cell Ω' is defined

$$\Omega' = \left\{ q_1\mathbf{k}_1 + q_2\mathbf{k}_2 : q_j \in [-\frac{1}{2}, \frac{1}{2}) \right\}.$$

This is also called the Brillouin zone. It is noted that Brillouin zone has other representations but all representations are the same due to the periodicity [42].

3 Honeycomb Lattices and Bloch Theory

A honeycomb lattice is a special 2-D lattice. Its unit cell is equivalent to a hexagon under discrete translational symmetries and all sites (local minima of the continuous periodic potential) are located at the vertices of this hexagon. Note that only two of these six vertices are independent under discrete translational symmetries. It also should be noted that a triangular lattice has a hexagonal structure as well but it has only one independent starting site which is located at the center. A triangular lattice only has one site per cell and all sites are identical.

By considering the site distribution, a honeycomb lattice is composed of two triangular sublattices. Namely there are two initial points $\mathbf{A} \in \Omega$ and $\mathbf{B} \in \Omega$, where $\mathbf{A} \neq \mathbf{B}$; then the two sublattices are

$$\Gamma_{\mathbf{A}} = \mathbf{A} + \Gamma; \qquad \Gamma_{\mathbf{B}} = \mathbf{B} + \Gamma$$

A honeycomb lattice is the union of the two sublattices, i.e.,

$$\Gamma_{\mathbf{H}} = \Gamma_{\mathbf{A}} \cup \Gamma_{\mathbf{B}}.$$

A honeycomb lattice and corresponding indices used herein are displayed in Fig. 1; we note that in the strong potential limit which we will consider there are coefficients ρ and ρ_0 that arise in the dispersion structure of the linear lattice; they are usually termed nearest neighbor hopping energies. In this paper we take $\rho_0 = 1$. The filled black dots are $\mathbf{A}$ lattice points and the circles are $\mathbf{B}$ lattice points. We see that an $\mathbf{A}$ lattice point $\mathbf{A_p} \in \Gamma_{\mathbf{A}}$ has three nearest neighbors that are all $\mathbf{B}$ lattice points: $\mathbf{B_p}, \mathbf{B_{p-v_1}}$ and $\mathbf{B_{p-v_2}}$; a $\mathbf{B}$ lattice point has three nearest neighbors that are all $\mathbf{A}$ lattice points: $\mathbf{A_p}, \mathbf{A_{p+v_1}}$ and $\mathbf{A_{p+v_2}}$.

Here we choose the following characteristic vectors of the honeycomb lattice

$$\mathbf{v}_1 = l\left(\frac{\sqrt{3}}{2}, \frac{1}{2}\right), \qquad \mathbf{v}_2 = l\left(\frac{\sqrt{3}}{2}, -\frac{1}{2}\right),$$
$$\mathbf{k}_1 = \frac{4\pi}{l\sqrt{3}}\left(\frac{1}{2}, \frac{\sqrt{3}}{2}\right), \qquad \mathbf{k}_2 = \frac{4\pi}{l\sqrt{3}}\left(\frac{1}{2}, -\frac{\sqrt{3}}{2}\right),$$

where l is the lattice constant.

If the wave intensity $|\psi(z, \mathbf{r})|$ is infinitesimal, the nonlinear term can be omitted and we get a linear Schrödinger equation with a periodic potential. Certain key

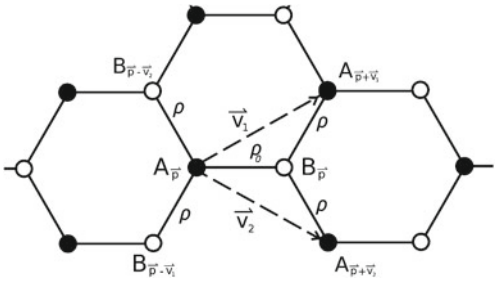

Fig. 1 A honeycomb lattice is composed of two triangular sublattices, $\Gamma_{\mathbf{A}}$ (*dots*) and $\Gamma_{\mathbf{B}}$ (*circles*), generated by $\mathbf{v}_1$ and $\mathbf{v}_2$ from different starting points. ρ and ρ_0 are coefficients associated with the dispersion structure of the linear lattice; they are usually termed nearest neighbor hopping energies; here we take $\rho_0 = 1$

solutions are obtained by considering $\psi(z, \mathbf{r}) = \varphi(\mathbf{r})e^{-i\mu z}$, where μ is constant. Then we obtain a linear eigenvalue problem

$$\left(-\nabla^2 + \delta V(\mathbf{r})\right)\varphi = \mu\varphi. \tag{2}$$

According to Bloch's theorem [43], the eigenfunction of the the eigenvalue problem (2), called the Bloch mode or the Bloch wave, has the $\mathbf{k}$-dependent form

$$\varphi(\mathbf{r}; \mathbf{k}) = e^{i\mathbf{k}\cdot\mathbf{r}}u(\mathbf{r}; \mathbf{k}) \tag{3}$$

where $u(\mathbf{r}; \mathbf{k})$ has the same periodicity as the potential $V(\mathbf{r})$ for any $\mathbf{k}$, i.e., $u(\mathbf{r} + \mathbf{v}; \mathbf{k}) = u(\mathbf{r}; \mathbf{k})$ for $\mathbf{v} \in \Gamma$. The eigenvalue $\mu = \mu(\mathbf{k})$ is referred to the dispersion relation.

Since the Bloch mode φ is usually not periodic in $\mathbf{r}$, it is more convenient to study $u(\mathbf{r}; \mathbf{k})$ (instead of $\varphi(\mathbf{r}; \mathbf{k})$) where $u(\mathbf{r}; \mathbf{k}) \in L^2_{per}(\Omega)$. The following eigenvalue problem arises

$$\mathcal{H}_{\mathbf{k}}u^{(n)}(\mathbf{r}; \mathbf{k}) = \mu^{(n)}(\mathbf{k})u^{(n)}(\mathbf{r}; \mathbf{k}), n \geq 1 \tag{4}$$

where the operator $\mathcal{H}_{\mathbf{k}}$ is defined as

$$\mathcal{H}_{\mathbf{k}} = -\nabla^2 - 2i\mathbf{k} \cdot \nabla + |\mathbf{k}|^2 + \delta V(\mathbf{r}). \tag{5}$$

The spectrum of the operator $\mathcal{H}_{\mathbf{k}}$ is discrete [43], i.e.,

$$\sigma(\mathcal{H}_{\mathbf{k}}) = \bigcup_{n \geq 1} \mu^{(n)}(\mathbf{k}),$$

and they can be ordered as

$$\mu^{(1)}(\mathbf{k}) \leq \mu^{(2)}(\mathbf{k}) \leq \mu^{(3)}(\mathbf{k}) \leq \cdots.$$

$\mu^{(n)}(\mathbf{k})$ is continuous as a function of $\mathbf{k}$ and due to the gauge invariance $\mu^{(n)}(\mathbf{k})$ is periodic. As $\mathbf{k}$ varies in the Brillouin zone Ω', $\mu^{(n)}(\mathbf{k})$ sweep out a closed interval

which is called the nth, $n = 1, 2, 3...$ band of the dispersion relation. In the literature, a dispersion band is often referred as the entire continuous region which supports bounded Bloch modes, i.e., the whole interval between two adjacent regions where bounded Bloch modes are not allowed. In this context, a dispersion band can have multiple branches. Generally, the lowest band in the tight-binding limit is usually simple and well-separated from higher bands. However, due to the underlying symmetries honeycomb lattices may have degenerate ground states.

If the eigenvalue problem (2) can be solved completely, i.e., the dispersion relation $\mu(\mathbf{k})$ and associated Bloch waves can be constructed, the general linear problem can then be solved by a Bloch decomposition; this is due to the completeness of the Bloch waves in $L^2(\mathbb{R}^2)$; furthermore each Bloch mode propagates independently. However, it is usually not possible to construct the dispersion relation and associated Bloch waves analytically. Hence numerical and asymptotic approximations are usually used. There are various numerical schemes that can be used to solve this eigenvalue problem; e.g., finite differences and spectral methods are often utilized [44]. On the other hand, asymptotic approximations require some asymptotic limits. Two typical limits are $\delta \ll 1$ and $\delta \gg 1$ where the former case is sometimes referred as the low contrast limit (or shallow potential) and the latter case high contrast limit, or more often, tight-binding limit. If $\delta \ll 1$, direct perturbation theory of the eigenvalue problem can be carried out and $u(\mathbf{r}; \mathbf{k})$ can be obtained. The dispersion relation is obtained via solvability conditions; see [13] for example. If $\delta \gg 1$, an orbital approximation can be employed. In this case, the Bloch waves are localized around the wells and can be approximated by appropriate superposition of the orbitals. From the orbital approximation one can find the dispersion relation.

4 Nonlinear Discrete Dynamics

In the tight-binding limit ($\delta \gg 1$), the Bloch waves are localized around the sites and their main properties are determined from the potential in the vicinities of the wells. We introduce two single-well potentials $W_A(\mathbf{r})$ and $W_B(\mathbf{r})$ which approach $\max\{V(\mathbf{r}) : \mathbf{r} \in \Omega\}$ rapidly as $|\mathbf{r}| \to \infty$ and coincide with $V(\mathbf{r})$ in the vicinities of $\mathbf{A}$ and $\mathbf{B}$ respectively.

The orbitals ϕ_A and ϕ_B are defined as the eigenfunctions of the one-well potentials; namely,

$$\left(-\nabla^2 + \delta W_j(\mathbf{r})\right)\phi_j(\mathbf{r}) = E_j\phi_j(\mathbf{r}) \quad j = A, B \tag{6}$$

where E_j are the orbital energies. For simplicity, we let $W_A(\mathbf{r}) = W_B(\mathbf{r} - \mathbf{d})$ where $\mathbf{d}$ is the shift vector from $\mathbf{A}$ site to the $\mathbf{B}$ site in the same cell, then $E_A = E_B = E$. It is noted that the eigenvalue problem can have multiple discrete eigenvalues. We are only interested in the ground (or lowest) state which in turn gives the lowest band of the dispersion relation and determines the associated dynamics of the

honeycomb lattice. For these single-well potentials $W_A(\mathbf{r})$, the ground state is simple and the orbital energy E is well-separated from the excited energies on the order of $O(\sqrt{\delta})$ (cf. [45] and references therein).

Then the Bloch waves associated with the lowest band can be approximated by

$$\varphi(\mathbf{r};\mathbf{k}) = \sum_{\mathbf{v}} (\alpha(\mathbf{k})\phi_A(\mathbf{r}-\mathbf{v}) + \beta(\mathbf{k})\phi_B(\mathbf{r}-\mathbf{v}))e^{i\mathbf{k}\cdot\mathbf{v}}, \tag{7}$$

where $\alpha(\mathbf{k})$ and $\beta(\mathbf{k})$ are determined later by the original eigenvalue problem (2).

Substituting the above expression into eigenvalue problem (2) leads to a matrix eigenvalue problem where $(\alpha(\mathbf{k}), \beta(\mathbf{k}))$ is the eigenvector. The orbital approximation converts the eigenvalue problem of a differential operator to an eigenvalue problem of a 2×2 matrix. Since the discrete envelope equation, which will be obtained later in this section, inherits the dispersion relation of the eigenvalue problem (4) in the tight-binding limit, the direct derivation of the dispersion relation is omitted here. We explain later how to get the discrete dispersion relation in the following section where the full dispersion relation is given—see Eqs. (17)–(18a, b). Additional details can be found in [15].

The aim of this section is to understand the key equations which govern the dynamics of the wave packets associated with the lowest band. It turns out that the dispersion relation are exactly related to the linear part of the governing equation of the wave packets. The set $\{(\phi_A(\mathbf{r}-\mathbf{v}), \phi_B(\mathbf{r}-\mathbf{v}))\}_{\mathbf{v}\in\Gamma}$ can approximate the wave packets associated with the lowest band in the sense that

$$\psi(\mathbf{r}) = \sum_{\mathbf{v}} (A_{\mathbf{v}}\phi_A(\mathbf{r}-\mathbf{v}) + B_{\mathbf{v}}\phi_B(\mathbf{r}-\mathbf{v})). \tag{8}$$

In other words, $\{(A_{\mathbf{v}}, B_{\mathbf{v}})\}_{\mathbf{v}\in\Gamma} \in l^2(\Gamma)$ is a natural representation of the continuous $L^2(\mathbb{R}^2)$ envelope associated with the lowest band and $\{(\phi_A(\mathbf{r}-\mathbf{v}), \phi_B(\mathbf{r}-\mathbf{v}))\}_{\mathbf{v}\in\Gamma}$ plays the role of a basis. This decomposition is sometimes referred as coupled mode theory [11].

The above decomposition (8) is similar to a Wannier decomposition (see for example [46]). But orbitals and Wannier functions are not the same. Wannier functions are the Fourier coefficients of the Bloch modes $\varphi(\mathbf{r};\mathbf{k})$ which are periodic functions in $\mathbf{k}$. Hence they are only defined in periodic lattices. On the other hand in the tight-binding limit orbitals are natural approximations to eigenfunctions associated with complicated potentials and this is not necessarily limited to periodic potentials. The definition of the orbital is straightforward and leads to physical insight and intuition. In simple lattices, orbitals can be used as the approximations to the Wannier functions; but in many cases Wannier functions can be employed directly. However, in non-simple lattices, Wannier functions are difficult to construct and their interactions are complicated.

Substituting the above wave packet approximation (8) into the lattice NLS Eq. (1) implies

$$\sum_{\mathbf{v}}\left(i\frac{dA_{\mathbf{v}}}{dz}+A_{\mathbf{v}}\delta(V(\mathbf{r})-W_A(\mathbf{r}-\mathbf{v}))\right)\phi_A(\mathbf{r}-\mathbf{v})$$
$$+\sum_{\mathbf{v}}\left(i\frac{dB_{\mathbf{v}}}{dZ}+B_{\mathbf{v}}\delta(V(\mathbf{r})-W_B(\mathbf{r}-\mathbf{v})\right)\phi_B(\mathbf{r}-\mathbf{v})$$
$$+\sigma\left(\sum_{\mathbf{v}}(A_{\mathbf{v}}\phi_A(\mathbf{r}-\mathbf{v})+B_{\mathbf{v}}\phi_A(\mathbf{r}-\mathbf{v}))\right)^2$$
$$\times\left(\sum_{\mathbf{v}}(A_{\mathbf{v}}\phi_A(\mathbf{r}-\mathbf{v})+B_{\mathbf{v}}\phi_B(\mathbf{r}-\mathbf{v}))\right)^*=0. \tag{9}$$

Multiplying both sides by $\phi_A(\mathbf{r}-\mathbf{p})$ and $\phi_B(\mathbf{r}-\mathbf{p})$ respectively and integrating lead to (only nearest neighbor interaction terms are kept)

$$i\frac{dA_{\mathbf{p}}}{dz}+c_0A_{\mathbf{p}}+(\tau\mathcal{L}^-)B_{\mathbf{p}}+\sigma g|A_{\mathbf{p}}|^2A_{\mathbf{p}}=0,$$
$$i\frac{dB_{\mathbf{p}}}{dz}+c_0B_{\mathbf{p}}+(\tau\mathcal{L}^+)A_{\mathbf{p}}+\sigma g|B_{\mathbf{p}}|^2B_{\mathbf{p}}=0,$$

where $c_0=\int\phi_A(\mathbf{r})\delta(V(\mathbf{r})-W_A(\mathbf{r}))\phi_A d\mathbf{r}$, $\tau=\int\phi_A(\mathbf{r})\delta(V(\mathbf{r})-W_A(\mathbf{r}-\mathbf{v}))\phi_A(\mathbf{r})d\mathbf{r}$, $g=\int\phi_A^4 d\mathbf{r}$,

$$\mathcal{L}^-B_{\mathbf{p}}=B_{\mathbf{p}}+\rho_1B_{\mathbf{p}-\mathbf{v}_1}+\rho_2B_{\mathbf{p}-\mathbf{v}_2}, \tag{10}$$

$$\mathcal{L}^+A_{\mathbf{p}}=A_{\mathbf{p}}+\rho_1A_{\mathbf{p}+\mathbf{v}_1}+\rho_2A_{\mathbf{p}+\mathbf{v}_2}, \tag{11}$$

and $\rho_j=\frac{1}{\tau}\int\phi_A(\mathbf{r})\delta(V(\mathbf{r})-W_A(\mathbf{r}))\phi_A(\mathbf{r}-\mathbf{v}_j)d\mathbf{r}$, $j=1,2$. Here c_0 represents the correction to the orbital energy due to the difference between the orbital potentials and the lattice potentials, τ is the magnitude of the nearest neighbor hopping energy while ρ_1 and ρ_2 represent the inequality of the three nearest neighbor hopping energies. This inequality measures the deformation of the honeycomb lattice. If $\rho_1=\rho_2=1$, the honeycomb lattice is undeformed. The deformation is induced by the inequality of distances of any given site to its three nearest neighbors. It can also be induced by other reasons, for example, local doping to change the depth of wells and so on. For simplicity, we take $\rho_1=\rho_2$. More detailed calculations of these parameters can be found in [15].

Rewriting the discrete system, we have the following rescaled couple-mode equation

$$i\frac{dA_{\mathbf{p}}}{dz}+\mathcal{L}^-B_{\mathbf{p}}+\sigma|A_{\mathbf{p}}|^2A_{\mathbf{p}}=0, \tag{12}$$

$$i\frac{dB_{\mathbf{p}}}{dz}+\mathcal{L}^+A_{\mathbf{p}}+\sigma|B_{\mathbf{p}}|^2B_{\mathbf{p}}=0. \tag{13}$$

It governs the evolution of Bloch waves associated with the lowest band. This coupled mode equation is different from the 2-D discrete NLS equation associated with simple lattices. A significant difference is that this couple mode equation contains two equations which come from the non-equivalence of **A** and **B** sites. This coupled mode equation governs the dynamics of the wave packets associated with the whole lowest band.

If an envelope is associated with a specific wave number **k**, then it can be conveniently represented by

$$\psi(\mathbf{r}) \approx \sum_{\mathbf{p}\in\Gamma} \big(a_{\mathbf{p}}\phi_A(\mathbf{r}-\mathbf{p}) + b_{\mathbf{p}}\phi_B(\mathbf{r}-\mathbf{p})\big)e^{i\mathbf{k}\cdot\mathbf{p}}.$$

A single-mode equation is then obtained. For completeness we also give the equations of the discrete envelope in terms of the variables $\{(a_{\mathbf{p}}(z), b_{\mathbf{p}}(z))\}_{\mathbf{p}\in\Gamma}$ (see [15])

$$i\frac{da_{\mathbf{p}}}{dz} + \mathcal{L}_{\mathbf{k}}^{-} b_{\mathbf{p}} + \sigma|a_{\mathbf{p}}|^2 a_{\mathbf{p}} = 0, \tag{14a}$$

$$i\frac{db_{\mathbf{p}}}{dz} + \mathcal{L}_{\mathbf{k}}^{+} a_{\mathbf{p}} + \sigma|b_{\mathbf{p}}|^2 b_{\mathbf{p}} = 0, \tag{14b}$$

where

$$\mathcal{L}_{\mathbf{k}}^{-} b_{\mathbf{p}} = b_{\mathbf{p}} + \rho b_{\mathbf{p}-\mathbf{v}_1} e^{-i\mathbf{k}\cdot\mathbf{v}_1} + \rho b_{\mathbf{p}-\mathbf{v}_2} e^{-i\mathbf{k}\cdot\mathbf{v}_2},$$
$$\mathcal{L}_{\mathbf{k}}^{+} a_{\mathbf{p}} = a_{\mathbf{p}} + \rho a_{\mathbf{p}+\mathbf{v}_1} e^{i\mathbf{k}\cdot\mathbf{v}_1} + \rho a_{\mathbf{p}+\mathbf{v}_2} e^{i\mathbf{k}\cdot\mathbf{v}_2}.$$

It is noted that the single-mode Eq. (14a, b) can be obtained from Eq. (12) by changing $(A_{\mathbf{p}}, B_{\mathbf{p}})$ to $(a_{\mathbf{p}}e^{i\mathbf{k}\cdot\mathbf{p}}, b_{\mathbf{p}}e^{i\mathbf{k}\cdot\mathbf{p}})$. This is due to the linear properties of the coupled mode equation which will be discussed in the next section. It should also be noted that the above discrete approach can be extended beyond the tight binding limit. If the potential intensity δ is not sufficiently large, the nearest neighbor interaction approximation may not be adequate. In such cases additional sites should be included in order to get more accurate approximations. A rigorous discussion for the validity of the orbital approximation can be found in [45].

5 Linear Properties

Neglecting the nonlinear terms in (12), the linear equation can be solved by using a discrete Fourier transform, i.e.,

$$\hat{A}(\mathbf{k}; z) = \sum_{\mathbf{v}\in\Gamma} A_{\mathbf{v}} e^{-i\mathbf{k}\cdot\mathbf{v}}, \quad A_{\mathbf{v}} = \frac{1}{|\Omega'|}\int_{\Omega'} \hat{A}(\mathbf{k}) e^{i\mathbf{k}\cdot\mathbf{v}} d\mathbf{k},$$

where $|\Omega'|$ is the area of Ω'.

Similar to what is indicated above, substituting the Fourier mode $\{(\hat{A}(\mathbf{k}), \hat{B}(\mathbf{k}))e^{-i\omega z+i\mathbf{k}\cdot\mathbf{v}}\}_{\mathbf{v}\in\Gamma}$ into the linear discrete evolution problem associated with Eq. (12) leads to

$$\begin{pmatrix} \omega & \gamma(\mathbf{k}) \\ \gamma^*(\mathbf{k}) & \omega \end{pmatrix} \begin{pmatrix} \hat{A}(\mathbf{k}) \\ \hat{B}(\mathbf{k}) \end{pmatrix} = \begin{pmatrix} 0 \\ 0 \end{pmatrix}, \tag{15}$$

where $\gamma(\mathbf{k}) = 1 + \rho e^{-i\mathbf{k}\cdot\mathbf{v}_1} + \rho e^{-i\mathbf{k}\cdot\mathbf{v}_2}$. Unlike the continuous Fourier transform, in the discrete Fourier transform $\mathbf{k}$ only takes values in Ω' as opposed to all of $\mathbb{R}^2$. Existence of nontrivial solutions leads to the dispersion relation $\omega(\mathbf{k})$ which is only defined in the Brillouin zone Ω'; In other words, the dispersion relation $\omega(\mathbf{k})$ is continuous and periodic with two periods $\mathbf{k}_1$ and $\mathbf{k}_2$ in $\mathbb{R}^2$. This dispersion relation $\omega(\mathbf{k})$ approximates the original dispersion relation $\mu(\mathbf{k})$ apart from scalings; namely,

$$\mu(\mathbf{k}) = E + c_0 + \tau\omega(\mathbf{k}) \tag{16}$$

where we recall that E is the orbital energy which is mainly determined by the potential in the vicinity of a site; c_0 is the correction to the orbital energy which is from the difference between the lattice potential and the approximating orbital potential; as indicated above τ is the magnitude of the nearest neighbor hopping energy which represents the strength of the interactions between sites; $\omega(\mathbf{k})$ is the effective dispersion relation. The corresponding Bloch modes can then be constructed from Eq. (7) where $(\alpha(\mathbf{k}), \beta(\mathbf{k}))$ are the eigenvectors of (15). Hence the coupled mode equation inherits the dispersion relation of the original lattice NLS equation. In our case, existence of nontrivial solutions to (15) leads

$$\omega_\pm(\mathbf{k}) = \pm\left|1 + \rho e^{-i\mathbf{k}\cdot\mathbf{v}_1} + \rho e^{-i\mathbf{k}\cdot\mathbf{v}_2}\right|. \tag{17}$$

We see that the dispersion relation has two branches: $\omega_+(\mathbf{k}) = -\omega_-(\mathbf{k})$. The two branches may or may not intersect with each other depending on the value of ρ. Let $\mathbf{K}_* = \mathbf{K}_*(\rho) \in \Omega'$ denote the special point(s) in the Brillouin zone such that $\omega_+(\mathbf{K}_*) = \min_{\mathbf{k}\in\Omega'}\omega_+(\mathbf{k})$, and, $\omega_-(\mathbf{K}_*) = \max_{\mathbf{k}\in\Omega'}\omega_-(\mathbf{k})$. The values, $(\mathbf{K}_*, \omega_\pm(\mathbf{K}_*))$ are the closest values of the two branches if there is a gap between them. If the two branches intersect, $\omega_+(\mathbf{K}_*) = \omega_-(\mathbf{K}_*) = 0$ and $(\mathbf{K}_*, \omega_\pm(\mathbf{K}_*))$ are the intersection points.

Calling $\beta = 2\rho - 1$, a direct calculation shows that

1. If $\beta > 0$, the two branches touch each other at two different points which are referred as the Dirac points. Namely, $\mathbf{K}_*$ has two values in entire the Brillouin zone Ω': $\mathbf{K}_* = \pm\mathbf{K} = \pm\frac{2}{l}\left(0, \pi - \arccos(\frac{1}{2\rho})\right)$. Near the $\mathbf{K}$ point, the dispersion relation has the leading expansion $\omega_\pm(\mathbf{K}+\mathbf{q}) \sim \pm\sqrt{q_1^2 + (\beta^2+2\beta)q_2^2}$ where $\mathbf{q} = (q_1, q_2)$ and $|\mathbf{q}| \ll 1$ which forms a local elliptic cone.

2. If $\beta = 0$, the two branches touch each other at one point. In this critical case, the two Dirac points actually merge into one due to the underlying periodicity of $\mathbf{k} \in \mathbb{R}^2$. Namely, $\mathbf{K} \to \frac{2}{l}(0, \pi) = \frac{1}{2}(\mathbf{k}_1 - \mathbf{k}_2)$ as $\rho \to \frac{1}{2}$, and both $\frac{1}{2}(\mathbf{k}_1 - \mathbf{k}_2)$ and $-\frac{1}{2}(\mathbf{k}_1 - \mathbf{k}_2)$ are equivalent to $\frac{1}{2}(-\mathbf{k}_1 - \mathbf{k}_2) \in \Omega'$ due to the periodicity. Near the intersection point $\mathbf{K}_*$, the dispersion relation has the leading expansion $\omega_\pm(\mathbf{K}_* + \mathbf{q}) \sim \pm |q_1|$ where $\mathbf{q} = (q_1, q_2)$ and $|\mathbf{q}| \ll 1$ which is the degeneration of the above ellipse to local crossing of planes.
3. If $\beta < 0$, the two branches separate from each other and there exists a gap between the two branches. The only closest point is $\mathbf{K}_* = \frac{1}{2}(-\mathbf{k}_1 - \mathbf{k}_2) = (\frac{4\pi}{l\sqrt{3}}, 0)$. Near $\mathbf{K}_*$ points, the dispersion relation has the leading expansion $\omega_\pm(\mathbf{K}_* + \mathbf{q}) \sim \pm \sqrt{\beta^2 + (1+\beta)^2 q_1^2}$ where $\mathbf{q} = (q_1, q_2)$ and $|\mathbf{q}| \ll 1$ which has the structure of a hyperboloid. The gap width is $2|\beta|$.

6 Conical Dirac Dynamics

In many applications, the dynamics of an envelope associated with a specific value of $\mathbf{k}$ is of interest. Then the Eq. (14a, b) are more convenient to use. From these equations we can derive a continuous system which is more convenient to study instead of the differential-difference equation.

The discrete envelope can be considered as the continuous envelope evaluated at the lattice points, i.e., $a_{\mathbf{p}}(z) = a(\mathbf{r} = \mathbf{p}, z)$ and $b_{\mathbf{p}}(z) = b(\mathbf{r} = \mathbf{p}, z)$; here the continuous transverse variable associated with the lattice is $\mathbf{r} = (r_1, r_2)$. In this application the envelopes are assumed to depend only on the long-wave variables and the amplitudes are assumed small. Accordingly, we define, $(a(\mathbf{r}, z), b(\mathbf{r}, z)) = \sqrt{v}(\tilde{a}(\mathbf{x}, \tilde{z}), \tilde{b}(\mathbf{x}, \tilde{z}))$ where the transverse variable is given by $\mathbf{x} = (x_1, x_2) = \mathbf{r}/L$, the propagation variable is $\tilde{z} = vz$, $v = \frac{\sqrt{3}\, l}{2L} \ll 1$, where the lattice size is l and the envelope scale L is much greater than l, i.e., $\frac{l}{L} \ll 1$. For simplicity, we drop the tildes on the top of a, b and z.

Here we are interested in the effective dynamics associated with the special point(s) $\mathbf{K}_*$. It turns out that if the initial envelope is associated with a value $\mathbf{k}$ which is far away from $\mathbf{K}_*$, then the continuous dynamics reduces to an effective nonlinear Schrödinger equation in a moving frame [15]. One can find effective NLS equations associated for simple bands; the lowest bands of most simple lattices also yield effective NLS equations. At $\mathbf{K}_*$, as β changes from positive to negative values, both the geometric structure of the dispersion relation and the associated effective wave dynamics change dramatically. We investigate some of the important cases next.

We first consider the case $\beta > 0$. As indicated above, the two branches touch each other at the Dirac points: $\mathbf{K}$ and $-\mathbf{K}$. Here we only consider the effective

dynamics associated with $\mathbf{K}$; the analysis for $-\mathbf{K}$ is similar. At $\mathbf{k} = \mathbf{K}$, $\omega_\pm = 0$ and by direct calculation we have

$$\rho e^{-i\mathbf{K}\cdot\mathbf{v}_1} + \rho e^{-i\mathbf{K}\cdot\mathbf{v}_2} = -1, \qquad \rho e^{-i\mathbf{K}\cdot\mathbf{v}_1} - \rho e^{-i\mathbf{K}\cdot\mathbf{v}_2} = -i\sqrt{4\rho^2 - 1}.$$

Calling $\zeta = \sqrt{4\rho^2 - 1} = \sqrt{\beta^2 + 2\beta}$ and using Taylor expansion, and evaluating at $\mathbf{k} = \mathbf{K}$, we have

$$\mathcal{L}_{\mathbf{K}}^{-} b_{\mathbf{p}} \sim v^{3/2}\left[(\partial_{x_1} + i\frac{\zeta}{\sqrt{3}}\partial_{x_2}) - \frac{v}{2}\left(\partial_{x_1}^2 + \frac{1}{3}\partial_{x_2}^2 + 2i\frac{\zeta}{\sqrt{3}}\partial_{x_1}\partial_{x_2}\right) + \frac{v^2}{6}\left(\partial_{x_1}^3 + \frac{1}{3\sqrt{3}}\partial_{x_2}^3 + \partial_{x_1}\partial_{x_2}^2 + \sqrt{3}i\zeta\partial_{x_1}^2\partial_{x_2}\right)\right] b + \cdots$$

and

$$\mathcal{L}_{\mathbf{K}}^{+} a_{\mathbf{p}} \sim v^{3/2}\left[(-\partial_{x_1} + i\frac{\zeta}{\sqrt{3}}\partial_{x_2}) - \frac{v}{2}\left(\partial_{x_1}^2 + \frac{1}{3}\partial_{x_2}^2 - 2i\frac{\zeta}{\sqrt{3}}\partial_{x_1}\partial_{x_2}\right) - \frac{v^2}{6}\left(\partial_{x_1}^3 + \frac{1}{3\sqrt{3}}\partial_{x_2}^3 + \partial_{x_1}\partial_{x_2}^2 - \sqrt{3}i\zeta\partial_{x_1}^2\partial_{x_2}\right)\right] a + \cdots$$

If $\beta = O(1)$, i.e., $\zeta = O(1)$, then only taking the leading order term, we immediately obtain the so-called nonlinear Dirac equation

$$i\partial_z a + \left(\partial_{x_1} + i\frac{\zeta}{\sqrt{3}}\partial_{x_2}\right) b + \sigma|a|^2 a = 0; \tag{18a}$$

$$i\partial_z b + \left(-\partial_{x_1} + i\frac{\zeta}{\sqrt{3}}\partial_{x_2}\right) a + \sigma|b|^2 b = 0. \tag{18b}$$

The above nonlinear Dirac equation describes the evolution of the wave packet in the vicinity of the Dirac points. It is seen that the linear dispersion relation of Eq. (18a, b) reveals the leading order expansion of the effective dispersion relation which is a double cone. Namely, $\omega_\pm(\mathbf{q}) = \pm\sqrt{q_1^2 + \frac{\zeta^2}{3}q_2^2}$. A typical phenomenon associated with this equation is the conical diffraction. It says a localized input evolves into expending rings and a cone forms in the direction of propagation in the crystal. Typical conical diffraction is illustrated in Fig. 2. The top panel shows the evolution of an initial Gaussian envelope at the Dirac point $\mathbf{K}$ and then at two different propagating distances. If the lattice is not deformed, i.e., $\rho = 1$, then $\zeta = \sqrt{4\rho^2 - 1} = \sqrt{3}$ and circular ring structures are obtained. Figure 2 shows a comparison between the circular conical diffraction in the NLS Eq. (1) and the approximate nonliner Dirac equation (18a, b). The initial condition for the NLS equation is a weak and wide Gaussion envelope multiplied by a Bloch wave associated with the Dirac point $\mathbf{K}$. The initial condition for the nonlinear Dirac equation (18a, b) is $a(z = 0) = e^{-x_1^2 - x_2^2}$ and $b(z = 0) = 0$.

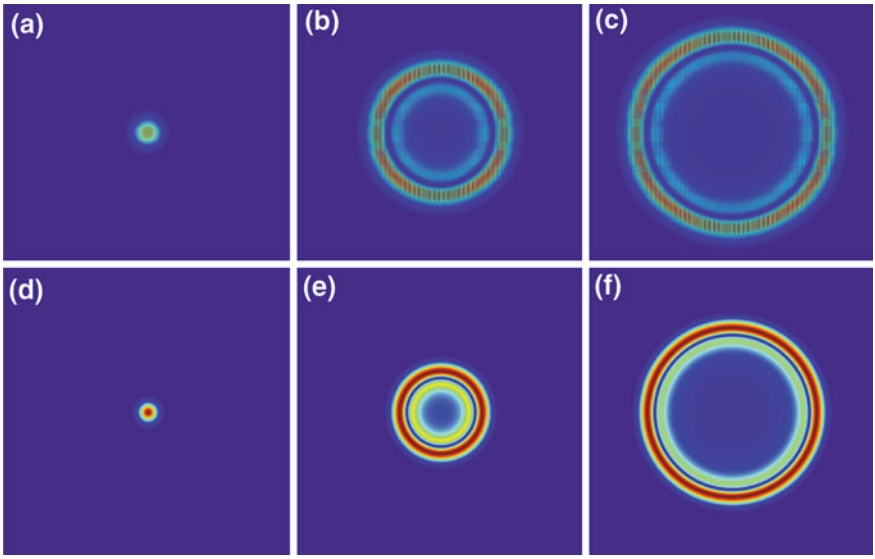

Fig. 2 Wave intensities initially a localized pulse (Gaussian) and subsequently at two successive propagating distances. *Top panel*: simulations of the lattice NLS equation (1). *Bottom panel*: simulations of the nonlinear Dirac equation (18a, b)

7 Symmetry Breaking and Nonlinear Transitions

Conical diffraction is a consequence of the behavior associated with a dispersion relation that has conical crossings. In principle it can be either linear and nonlinear; but as we will see with strong nonlinearity the conical behavior is modified. Next we analyze higher order dispersive effects and nonlinear transitions. It is found that the Dirac dynamics breaks down in the lattice NLS equation if the nonlinearity is strong [38]. As nonlinearity increases, the circular rings deform and become triangular. Figure 3 shows the evolution patterns for different nonlinear coefficients. It is noted that changing the value of σ is equivalent to changing the magnitude of the input.

Defining the operators $\mathcal{L}_0 = \begin{pmatrix} 0 & \partial_{x_1} + i\zeta\partial_{x_2} \\ -\partial_{x_1} + i\zeta\partial_{x_2} & 0 \end{pmatrix}$ and $\mathcal{L}_1 = \begin{pmatrix} 0 & \Delta_+ \\ \Delta_- & 0 \end{pmatrix}$, where $\Delta_\pm = \partial_{x_1}^2 + \frac{1}{3}\partial_{x_2}^2 \pm \frac{2}{\sqrt{3}} i\zeta\partial_{x_1}\partial_{x_2}$, we can write the higher order nonlinear Dirac equation in the following vector form

$$i\partial_z U + \mathcal{L}_0 U - \frac{v}{2}\mathcal{L}_1 U + N(U)U = 0 \tag{19}$$

where $U = (a, b)^T$ and the nonlinear operator is given by $N(U) = \begin{pmatrix} |a|^2 & 0 \\ 0 & |b|^2 \end{pmatrix}$.

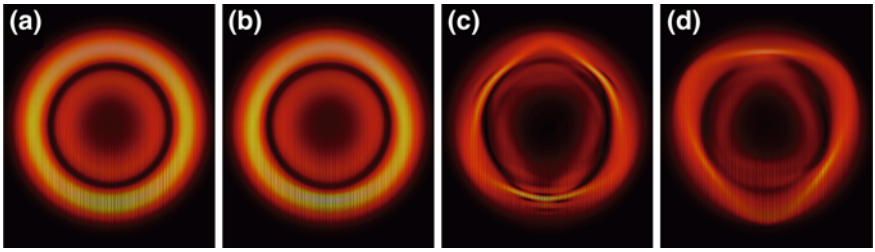

Fig. 3 Evolution patterns of the NLS equation (1) with nonlinear coefficient σ being: **a** 0; **b** 1; **c** 5; (**d**) −5. Here $v = 0.1$ and the evolution distance is $z = 50$ and $\delta = 100$ which is in the tight-binding regime

We first study the linear case. Define the Fourier transform $\mathcal{F}(F) = \hat{F} = \int F(\mathbf{x}) e^{-i\mathbf{q}\cdot\mathbf{r}} d\mathbf{x}$ and inverse Fourier transform $\mathcal{F}^{-1}(F) = \frac{1}{4\pi^2}\int F(\mathbf{q}) e^{i\mathbf{q}\cdot\mathbf{x}} d\mathbf{q}$. Note that $\mathbf{x} = (x_1, x_2)^T$ is the envelope coordinate, $\mathbf{q} = (q_1, q_2)^T$ is the wave number associated with the envelope, and from the above definitions the scales are different from $\mathbf{r}$ and $\mathbf{k}$ in the original lattice NLS Eq. (1).

Letting $\mathcal{L} = \mathcal{L}_0 - \frac{v}{2}\mathcal{L}_1$. Since $\mathcal{L}$ is a linear differential operator with constant coefficients, $\mathcal{F}(\mathcal{L}U) = \hat{\mathcal{L}}\hat{U}$ where $\hat{\mathcal{L}}$ is a 2×2 $\mathbf{k}$ $\mathbf{q}$-dependent matrix which has the form

$$\hat{\mathcal{L}} = \begin{pmatrix} 0 & iq_1 - q_2 \\ -iq_1 - q_2 & 0 \end{pmatrix} - \frac{1}{2}v \begin{pmatrix} 0 & -q_1^2 - \frac{1}{3}q_2^2 - \frac{2}{\sqrt{3}}i\zeta q_1 q_2 \\ -q_1^2 - \frac{1}{3}q_2^2 + \frac{2}{\sqrt{3}}i\zeta q_1 q_2 & 0 \end{pmatrix}.$$

We see that $\hat{\mathcal{L}}$ is a Hermitian matrix. In $\mathbf{q}$ space, the linear initial value problem becomes

$$i\hat{U}_z + \hat{\mathcal{L}}\hat{U} = 0, \hat{U}(z = 0) = \hat{U}_0.$$

Then we have

$$\hat{U}(z) = e^{i\hat{\mathcal{L}}z}\hat{U}_0.$$

$\hat{\mathcal{L}}$ has two eigenvalues $\omega_\pm(\mathbf{q}) = \pm q + O(v)$ which correspond to the two branches of the dispersion relation. The two branches intersect each other at the single point $\mathbf{q} = \mathbf{0}$. Note that at the degenerate point $\mathbf{q} = \mathbf{0}$, the multiplicity is two and for any $\mathbf{q}$ there are two linearly independent eigenvectors $\Phi_\pm$ which are normalized to be $\Phi_m^\dagger \Phi_n = \delta_{mn}$ where $m, n = +, -$. Hereafter, the superscript $\dagger$ means the complex conjugate with a transpose.

Then $\hat{\mathcal{L}} = (\Phi_+, \Phi_-)\Lambda(\Phi_+, \Phi_-)^\dagger$ where $\Lambda = \mathrm{diag}(\omega_1, \omega_2)$. Thus

$$\hat{U}(z) = (\Phi_+, \Phi_-)e^{i\Lambda z}(\Phi_+, \Phi_-)^\dagger \hat{U}_0$$

or rewriting

$$(\Phi_+, \Phi_-)^\dagger \hat{U}(z) = \mathrm{diag}(e^{i\omega_+ z}, e^{i\omega_- z})(\Phi_+, \Phi_-)^\dagger \hat{U}_0. \tag{20}$$

If we call $\hat{p}_\pm(z) = \Phi_\pm^\dagger \hat{U}(z)$, then $\hat{p}_\pm(z)$ represents the projection of $\hat{U}$ onto the $\pm$ branch in $\mathbf{q}$ space. From (20), we immediately obtain that

$$\hat{p}_\pm(z) = e^{i\omega_\pm z} p_\pm(z=0). \tag{21}$$

In addition we denote $\epsilon_\pm = \frac{1}{(2\pi)^2}\int |\hat{p}_\pm|^2 d\mathbf{k}$ which represents the energy associated with $\pm$ branch. From (21), we know that $\epsilon_\pm(z) = \epsilon_\pm(z=0)$. There is no energy exchange between two branches in the linear evolution.

Since (Φ_+, Φ_-) is unitary, the total energy of the system is given by

$$\begin{aligned}\epsilon(z) &= \int |U(\mathbf{r}, z)|^2 d\mathbf{r} = \frac{1}{(2\pi)^2}\int |\hat{U}(z)|^2 d\mathbf{k} = \frac{1}{(2\pi)^2}\int |(\Phi_+, \Phi_-)^\dagger \hat{U}|^2 d\mathbf{k} \\ &= \frac{1}{(2\pi)^2}\int |(\hat{p}_+, \hat{p}_-)^\dagger|^2 d\mathbf{k} = \epsilon_+(z) + \epsilon_-(z)\end{aligned}$$

where we have used Parseval's theorem.

The above analysis shows that: (i) the linear propagation can be decomposed into upper and lower components and each component evolves independently; (ii) the magnitudes of the projections of each branch remain the same under propagation—see Eq. (21).

We first focus on the combination of the higher order effects and nonlinearity without deformations. We take $\zeta = \sqrt{3}$ in the remainder of this section. The linear Dirac dynamics is essentially a 2-D wave equation after eliminating b and keeping a only or vice verse and it is a weakly dispersive system. Letting $q = |\mathbf{q}|$ and $\theta = \arctan(\frac{q_2}{q_1})$, then the dispersion relation has the form

$$\omega_\pm(q, \theta) = \pm q + O(v)$$

and the group velocities for $\mathbf{q} \neq \mathbf{0}$ are $\frac{\partial \omega_\pm}{\partial q} = \pm 1 + O(v)$, $\frac{\partial \omega_\pm}{\partial \theta} = 0 + O(v)$. Two eigenvectors have the form

$$\Phi_+ = \frac{1}{\sqrt{2}}\begin{pmatrix} e^{-i\frac{\theta}{2}} \\ ie^{i\frac{\theta}{2}} \end{pmatrix} + O(v), \quad \Phi_- = \frac{1}{\sqrt{2}}\begin{pmatrix} e^{-i\frac{\theta}{2}} \\ -ie^{i\frac{\theta}{2}} \end{pmatrix} + O(v).$$

Then to leading order, an initial localized input (e.g., a Gaussian spot) evolves into radially spreading rings. Along any specific angle θ, the field behaves like a traveling wave with unit velocity since the group velocity along θ direction is zero. The conical diffraction then ensues. Further, due to the preservation of the mass one expects that the intensity decays at the order of $O(\frac{1}{z})$. These conclusions can be deduced from long-time asymptotic methods.

Next we turn to the nonlinear and higher order dispersive effects. When higher order terms ($O(v)$ terms) are included, the dispersion relation is approximated by

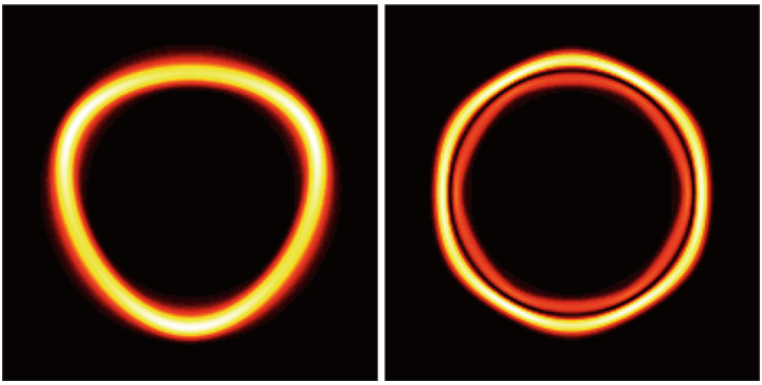

Fig. 4 Triangular and hexagonal patterns in the linear evolution of the HONLD Eq. (19). Here we take $v = 0.2$ to show higher order linear propagations

$$\omega_{\pm}(q,\theta) = \pm q(1 - \frac{v}{6} q \sin(3\theta)) + O(v^2) \tag{22}$$

we see that there is a three-fold symmetry. The dispersion $\omega_+(\mathbf{q})$ has three steepest descent directions and $\omega_-(\mathbf{q})$ has three orthogonal steepest descent directions. Each admits the so-called 'triangular warping'. If the initial condition is specified completely in one branch, the linear wave remains in that branch since there is no branch transition in the linear problem. In such a case a triangular pattern results. If initial condition is evenly distributed into the two branches, the patten is the superposition of two triangular patterns which evolves into a hexagonal shape. Figure 4 triangular and hexagonal patterns due to different initial conditions where $a(z=0) = e^{-x_1^2 - x_2^2}$ is a unit Gaussian and the choice of $b(z=0)$ for the left triangular figure is such that $\hat{p}_-(z=0) = 0$ and for the right hexagonal figure is $b(z=0) = 0$ which ensures $\hat{p}_-(z=0) = \hat{p}_+(z=0)$; i.e we take equal strength in both components. Here we choose $v = 0.2$ which corresponds to the strength of the higher order effects.

Nonlinearity brings two major effects. The first one is to couple the upper and lower branches together and the second one is to broaden $\hat{p}_{\pm}(z)$ in $\mathbf{q}$ space under propagation. Next we give some brief discussion on this matter. We first describe some numerical results for the HONLD equation. In the numerical simulations here, the initial input is always taken to be $a(x,y,0) = e^{-x^2-y^2}, b(x,y) = 0$ which ensures the two branches are initially evenly distributed. Figure 5 shows the evolution of such an input in the HONLD Eq. (19) for different σ. It is seen that a conical diffraction pattern changes into a triangular-like pattern as nonlinearity increases. This is consistent with Fig. 3. These results show that when the nonlinearity is significant the HONLD equation is needed in order to describe the envelope dynamics.

HONLD Eq. (19) is the single-mode equation which asymptotically describes the dynamics of the envelope associated with the Dirac point. Since the

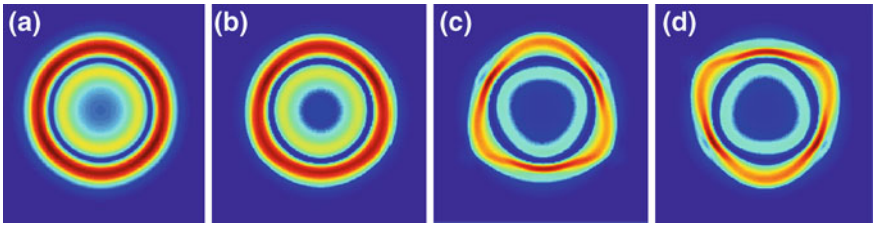

Fig. 5 Evolution patterns in the HONLD equation (19) with σ equal **a** 0; **b** 1; **c** 5, **d** -5. Here $v = 0.1$ and the evolution distance is $z = 5$

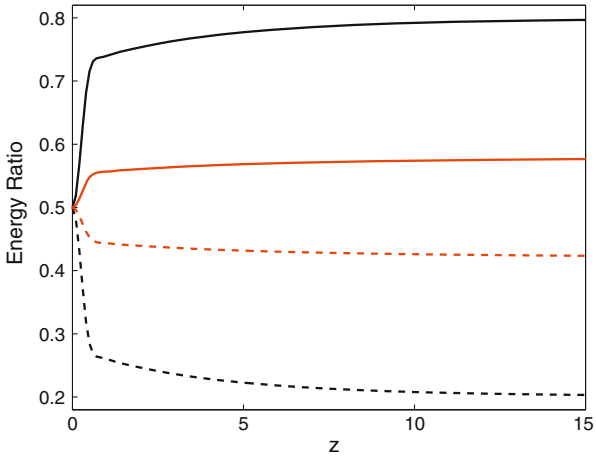

Fig. 6 The percentages of the energy in the two branches. The *black curves* are for $\sigma = 5$ and *red curves* for $\sigma = 1$; *dashed lines* for the lower branch and *solid lines* for the upper branch

nonlinearity is found to couple the two branches we plot the energy ratios of the two branches—see Fig. 6. It is seen that one branch is enhanced and the other is weakened. It is also seen that modifications to the energy ratios occur rapidly at the beginning and gradually saturates so that the percentages of the two branches tend to constant values. We reiterate that this occurs when the initial branches are taken to have the same energies.

Meanwhile, the projections $\hat{p_{\pm}}(z)$ also change under propagation. Figure 7 displays the changes of the projection $\hat{p}_+$ under propagation. It is seen that the energy spreads in $\mathbf{q}$ space. Since triangular warping increases as $|\mathbf{q}|$ increases, triangular diffraction become more noticeable. In order words, triangular warping breaks the radial symmetry of the circularly conical dispersion relation. This symmetry breaking is amplified when the nonlinearity is included.

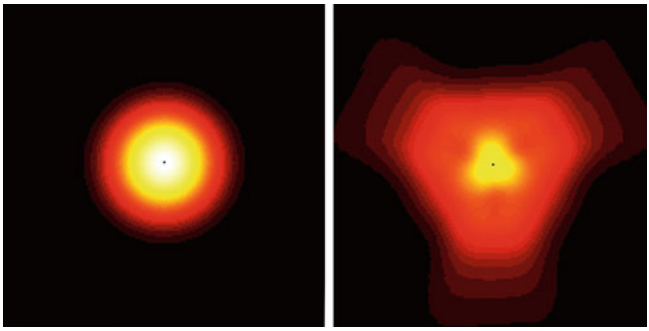

Fig. 7 The magnitude of the projection $\hat{p}_+(z)$ in the nonlinear evolution at $z = 0$ (*left*) and $z = 5$ (*right*). Here $\sigma = 5$

8 Effective Dynamics for Deformation Lattices

In applications, the honeycomb lattices are often not perfect. Deformations occur for many reasons such as local doping and uniform strains to the lattice. In such cases $\zeta \neq \sqrt{3}$ and $\beta \neq 1$. If the lattice is deformed slightly the diffraction is modified so that the circular rings now become elliptical in structure. Figure 8 shows such a deformation with elliptical conical diffraction. It is also noted that the energy is centralized to the x_1 direction of the ellipse. This is traced to the fact that $\frac{\partial \omega}{\partial \theta} \neq 0$ when $\zeta \neq \sqrt{3}$. Two steepest descent directions are $\theta = 0, \pi$. So the field is attracted to the horizontal axis.

However, in some cases, the deformation can be large enough so that the deformation parameter β becomes small enough to become comparable to the long wave parameter v. Then the dynamics changes considerably. When $|\beta| \ll 1$, the leading order equations is nearly a one-dimensional wave equation. In this case, instead of splitting to expanding rings, the localized input separates into two traveling waves.

Figure 9 displays such straight line diffraction patterns which are the simulations of the continuous equations of the coupled mode Eq. (14a, b) in two cases. The initial conditions are $a(z = 0) = x_1 e^{-x_1^2 - x_2^2}, b(z = 0) = 0$. This initial input ensures the regularity of the nonlocal equations we will derive later [47]. We see that the evolutions are degenerated into nearly straight line diffraction with some additional parabolic structures.

This section is devoted to understanding the effective dynamics along the moving frames. There are two small parameters noting: β and v. If they are comparable, various interesting maximally balanced equations and associated phenomena arise. We only illustrate a special balance $|\beta| = O(v^2)$ which has two subcases: $\beta > 0$ when the two branches still touch each other and $\beta < 0$ when a gap just opens.

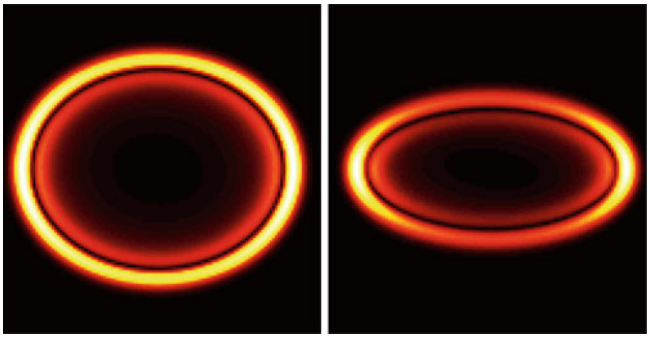

Fig. 8 Elliptical diffractions of the nonlinear Dirac equation (18a, b). *Left*: $\zeta = \frac{4\sqrt{3}}{5}$. *Right*: $\zeta = \frac{\sqrt{3}}{2}$

8.1 Before Separation

For simplicity, we introduce the variables $x = x_1, y = \frac{x_2}{\sqrt{3}}$. We then convert continuous system to a second order system which are linearly decoupled. Keeping terms up to $O(v^2)$ leads to

$$\partial_z^2 a - \partial_x^2 a + v^2 \mathcal{T}_{x,y} a + \sigma\Big[-i\partial_z(|a|^2 a) + \partial_x(|b|^2 b)\Big] = 0 \tag{23a}$$

$$\partial_z^2 b - \partial_x^2 b + v^2 \mathcal{T}_{x,y} b + \sigma\Big[-i\partial_z(|b|^2 b) - \partial_x(|a|^2 a)\Big] = 0 \tag{23b}$$

where

$$\mathcal{T}_{x,y} = -\alpha_1^2 \partial_y^2 + i\alpha_1(\partial_x^2 \partial_y - \partial_y^3) - \frac{1}{12}\left(\partial_x^4 + 6\partial_x^2\partial_y^2 - 3\partial_y^4 + 4\partial_x\partial_y^3\right)$$

and $\alpha_1 = \frac{\zeta}{v}$ which we assume is $O(1)$. Note that we only consider the case with weak nonlinearity, i.e., $|(a, b)| = O(v)$, some higher order terms in the nonlinear terms can be neglected in the above equation.

Accordingly, we introduce a slow time scale, $Z = v^2 z$ and we express a and b as

$$a = v(a_0(z, x, y, Z) + v^2 a_1(z, x, y, Z) + \cdots),$$
$$b = v(b_0(z, x, y, Z) + v^2 b_1(z, x, y, Z) \cdots)$$

where a_0 and b_0 satisfy the leading order equations and the dependence on z can be understood via the leading order equations while the dependence on Z will be given by the effective dynamics. Note that the only small parameter is v^2.

Define two moving frames, i.e., $\xi = x - z$ and $\eta = x + z$; hence a_0 and b_0 have the form

$$a_0 = F(\xi, y, Z) + G(\eta, y, Z)$$
$$b_0 = \tilde{F}(\xi, y, Z) + \tilde{G}(\eta, y, Z).$$

Furthermore, from the leading order equation we can easily get

Fig. 9 Diffraction patterns for large deformations. *Top*: $\beta = 0.005$ *Bottom*: $\beta = -0.01$. Here $v = 0.1$

$$\partial_\xi(-iF + \tilde{F}) = 0, \quad \partial_\eta(iG + \tilde{G}) = 0.$$

Hence for decaying functions: $\tilde{F} = iF$ and $\tilde{G} = -iG$.

At order $O(v^2)$, we have the equation

$$2\partial_\xi\partial_\eta a_1 = \mathcal{T}_{\xi,y}F + \mathcal{T}_{\eta,y}G + \left(-2\partial_\xi\partial_Z F + 2\partial_\eta\partial_Z G\right) + \sigma\Big[2i\partial_\xi(|F|^2F + 2|G|^2F + G^2F^*) - 2i\partial_\eta(|G|^2G + 2|F|^2G + F^2G^*)\Big];$$

When we integrate a_1, secular terms arise from the pieces that are functions of ξ or η alone, not both. Removal of secular terms at order $O(v^2)$ leads to the following maximally balanced nonlocal nonlinear equation for the right moving component

$$\partial_\xi\partial_Z F - \frac{1}{2}\mathcal{T}_{\xi,y}F - \sigma i\partial_\xi(|F|^2F) = 0, \tag{24}$$

and similarly the left moving component equation is

$$\partial_\eta\partial_Z G + \frac{1}{2}\mathcal{T}_{\eta,y}G - \sigma i\partial_\eta(|G|^2G) = 0.$$

We see that the above equations have a special nonlocal structure. The is reminiscent of the non-locality of the 2-D KP equation [41]. These equations are a two-dimensional NLS analog of the KP equation. We refer to them as NLSKP type equations. They describe the additional evolution structures along the moving frames. The simulation given in Fig. 10 shows the evolution given the initial data $F(\xi, y, Z = 0) = \xi e^{-\xi^2 - y^2}$, $\sigma = +1$. The additional structure obtained from the NLSKP Eq. (24) is consistent with Fig. 9; i.e. it is consistent with a blowup of the local structure depicted in Fig. 9.

8.2 After Separation

When $\beta < 0$, there is a gap between two dispersion branches. The edges to this gap for both branches are reached at $\mathbf{K}_* = -\frac{1}{2}\mathbf{k}_1 - \frac{1}{2}\mathbf{k}_2$. The width of the band gap is

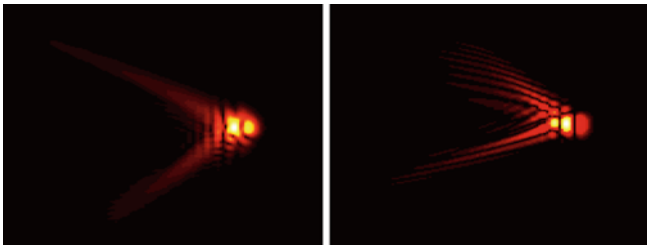

Fig. 10 Numerical simulations of NLSKP equations. *Left*: Eq. (24). *Right*: Eq. (26). Here $\sigma = +1$ and $\alpha_1 = \alpha_2 = 1$

$2|\beta|$. We then study the effective dynamics close to the edge; more specifically we study the case that $|\beta| = O(v^2)$ with $\alpha_2 = \frac{|\beta|}{v^2} = O(1)$.

It is noted that the continuous expansion changes when the gap is open. It is similar to the above case, so we omit the details. Taking the continuous limit from the discrete system (14a, b), making use of the relation: $\rho e^{-i\mathbf{K}_+\cdot\mathbf{v}_1} = \rho e^{-i\mathbf{K}_+\cdot\mathbf{v}_2} = -\rho$, keeping terms up to v^2 and rescaling the variables $x = x_1, y = x_2/\sqrt{3}$, we obtain the continuous equations

$$i\partial_z a + (1 - \alpha_2 v^2)\mathcal{F}_1 b + \alpha_2 v b + \sigma|a|^2 a = 0; \tag{25a}$$

$$i\partial_z b + (1 - \alpha_2 v^2)\mathcal{F}_2 a + \alpha_2 v a + \sigma|b|^2 b = 0; \tag{25b}$$

where

$$\mathcal{F}_1 = \partial_x - \frac{v}{2}(\partial_x^2 + \partial_y^2) + \frac{v^2}{6}\left(\partial_x^3 + \partial_y^3 + 3\partial_x\partial_y^2\right)$$
$$\mathcal{F}_2 = -\partial_x - \frac{v}{2}(\partial_x^2 + \partial_y^2) - \frac{v^2}{6}\left(\partial_x^3 + \partial_y^3 + 3\partial_x\partial_y^2\right).$$

As before we convert the above equations to a second order system which is of the form

$$\partial_z^2 a - \partial_x^2 a + v^2\mathcal{F}_{x,y}a + \sigma\left[-i\partial_t(|a|^2 a) + \partial_x(|b|^2 b)\right] = 0$$
$$\partial_z^2 b - \partial_x^2 b v^2\mathcal{F}_{x,y}b + \sigma\left[-i\partial_t(|b|^2 b) + \partial_x(|a|^2 a)\right] = 0,$$

where the operator

$$\mathcal{F}_{x,y} = \alpha_2^2 - \alpha_2(\partial_x^2 + \partial_y^2) - \frac{1}{12}\left(\partial_x^4 + 6\partial_x^2\partial_y^2 - 3\partial_y^4 + 4\partial_x\partial_y^3\right)$$

and we recall $\alpha_2 = \frac{|\beta|}{v^2}$ is $O(1)$.

Then we express a and b as

$$a = v(a_0(\xi, \eta, y, Z) + v^2 a_1(\xi, \eta, y, Z) + \cdots),$$
$$b = v(b_0(\xi, \eta, y, Z) + v^2 b_1(\xi, \eta, y, Z) + \cdots),$$

where a_0 and b_0 satisfy the leading order equations.

As above, a similar calculation shows that

$$a_0 = F(\xi, y, Z) + G(\eta, y, Z), \quad b_0 = iF(\xi, y, Z) - iG(\eta, y, Z).$$

At order $O(v^2)$, we have

$$2\partial_\xi\partial_\eta a_1 = \mathcal{F}_{\xi,y}F + \mathcal{F}_{\eta,y}G + \left(-2\partial_\xi\partial_Z F + 2\partial_\eta\partial_Z G\right) + \sigma\Big[2i\partial_\xi(|F|^2F + 2|G|^2F + G^2F^*) - 2i\partial_\eta(|G|^2G + 2|F|^2G + F^2G^*)\Big];$$

$\mathcal{F}_{\xi,y}$ and $\mathcal{F}_{\eta,y}$ are obtained from $\mathcal{F}_{x,y}$ by changing x to ξ and η respectively.

Removal of secular terms at order v^2 leads to two maximally balanced equations which govern the leading order dynamics of the right and left moving components; the equation for F is

$$\partial_\xi\partial_Z F - \frac{1}{2}\mathcal{F}_{\xi,y}F - \sigma i\partial_\xi(|F|^2F) = 0, \tag{26}$$

and the equation for G is

$$\partial_\eta\partial_Z G + \frac{1}{2}\mathcal{F}_{\eta,y}G - \sigma i\partial_\eta(|G|^2G) = 0.$$

These nonlocal equations are also NLSKP-type, though slightly different from those found the preceding subsection. In Fig. 10 we show a typical numerical result. We see similarity to the preceding case –see Eq. (24)—but with more of a focusing effect which is ascribed to our now being in the gap region.

9 Conclusion

Wave propagation in honeycomb lattices has attracted keen interest in many disciplines. This paper discusses nonlinear waves in honeycomb lattices and in particular nonlinear optical wave propagation are studied in deformed honeycomb lattices. Discrete coupled mode equations were obtained via an orbital approximation. These equations describe the lowest band of the linear dispersion relation of the original lattice NLS equation. Depending on the deformation, the dispersion relation may or may not admit conical crossings. In undeformed lattices, there are two Dirac cones. The associated envelope dynamics is obtained by taking the continuum limit of the couple mode equations near the Dirac points. This results in a higher order nonlinear Dirac equation. Utilizing this equation, both linear and nonlinear propagation of the envelope wave packets near Dirac points are analyzed. The leading order effect is a circular conical diffraction while the next order correction modifies the circular structure into hexagonal structure in the linear problem and triangular diffraction when nonlinearity is included. In general higher

order linear effects become noticeable even when v is very small. We see that nonlinearity expands the energy distribution in momentum space. In addition, nonlinearity also induces the coupling of two branches. Depending on the sign of the nonlinearity, one branch is enhanced while the other is weakened. Triangular diffraction is obtained even when initial condition is evenly distributed between the two branches.

When the deformation is small, the evolution pattern is changed moderately: circular conical diffraction becomes elliptical. However, when the deformation is large, the two branches may separate from each other and conical crossings in the dispersion relation disappear. In this regime a localized input splits into two moving nearly straight line components propagating in 'left and right' going directions. The effective dynamics of the wave packets associated with the Dirac point (before separation) or edge point (after separation) is described by into two maximally balanced nonlocal NLS equations termed here as: NLSKP type equations.

Acknowledgments Mark J. Ablowitz was partially supported by the U.S. Air Force Office of Scientific Research, under grant FA9550-12-0207 and by NSF under grants DMS-0905779, CHE 1125935. Yi Zhu was partially supported by the NSFC under grant 11204155.

References

1. K.S. Novoselov, A.K. Geim, S.V. Morozov, D. Jiang, Y. Zhang, S.V. Dubonos, I.V. Grigorieva, A.A. Firsov, Electric field effect in atomically thin carbon films. Science **306**, 666–669 (2004)
2. K.S. Novoselov, A.K. Geim, S.V. Morozov, D. Jiang, M.I. Katsnelson, I.V. Grigorieva, S.V. Dubonos, A.A. Firsov, Two-dimensional gas of massless Dirac fermions in graphene. Nature **438**, 197–200 (2005)
3. N.M.R. Peres, K.S. Novoselov, A.H. Castro Neto, F. Guinea, A.K. Geim, The electronic properties of graphene. Rev. Modern Phys. **81**, 109 (2009)
4. O. Peleg, G. Bartal, B. Freedman, O. Manela, M. Segev, D.N. Christodoulides, Conical diffraction and gap solitons in honeycomb photonic lattices. Phys. Rev. Lett. **98**, 103901 (2007)
5. O. Morsch, M. Oberthaler, Dynamics of bose-einstein condensates in optical lattices. Rev. Mod. Phys. **1**, 179–215 (2006)
6. S.L. Zhu, B. Wang, L.M Duan, Simulation and detection of Dirac fermions with cold atoms in an optical lattice. Phys. Rev. Lett. **98**, 260402 (2007)
7. Y.S. Kivshar, P. Agrawal Govind, *Optical Solitons: From Fibers to Photonic Crystals* (Academic press, San Diego, 2003)
8. M.I. Carvalho, S.R. Singh, D.N. Christodoulides, Vector interactions of steady-state planar solitons in biased photorefractive media. Opt. Lett. **20**, 2177–2179 (1995)
9. M. Segev, N.K. Efremidis, J.W. Fleisher, T. Carmon, D.N. Christodoulides, Observation of discrete solitons in optically induced real time waveguide arrays. Phys. Rev. Lett. **90**, 023902 (2003)
10. N.K Efremidis, J.W. Fleisher, M. Segev, D.N. Christodoulides, Observation of two-dimensional discrete solitons in optically induced nonlinear photonic lattices. Nature **422**, 147 (2003)

11. D.N. Christodoulides, R.J. Joseph, Discrete self-focusing in nonlinear arrays of coupled waveguides. Opt. Lett. **13**, 794–796 (1988)
12. P.G. Kevrekidis, B.A. Malomed, Y.B. Gaididei, Solitons in triangular and honeycomb dynamical lattices with the cubic nonlinearity. Phys. Rev. E **66**, 016609 (2002)
13. M.J. Ablowitz, Y. Zhu, Unified description of the dynamics of wave envelopes in two-dimensional simple periodic lattices. Stud. Appl. Math. (to appear)
14. M. Ablowitz, S. Nixon, Y. Zhu, Conical diffraction in honeycomb lattices. Phys. Rev. A **79**, 053830 (2009)
15. M.J. Ablowitz, Y. Zhu, Evolution of bloch-mode envelopes in two-dimensional generalized honeycomb lattices. Phys. Rev. A **82**, 013840 (2010)
16. L.H. Haddad, L.C. Carr, The nonlinear Dirac equation in bose-einstein condensates: foundation and symmetries. Physica D **238**, 1413–1421 (2009)
17. A.B. Aceves, B. Costantini, C. De Angelis, Two-dimensional gap solitons in a nonlinear periodic slab waveguide. J. Opt. Soc. Am. B **12**, 1475–1479 (1995)
18. J.K. Yang, I. Makasyuk, A. Bezryadina, Z. Chen, Dipole solitons in optically induced two-dimensional photonic lattices. Opt. Lett. **29**, 1662–1664 (2004)
19. D.N. Neshev, T.J. Alexander, E.A. Ostrovskaya, Y.S. Kivshar, I. Martin, H. Makasyuk, Z.G. Chen, Observation of discrete vortex solitons in optically induced photonic lattices. Phys. Rev. Lett. **92**, 123903 (2004)
20. X. Wang, Z. Chen, J. Wang, J. Yang, Observation of in-band lattice solitons. Phys. Rev. Lett. **99**, 243901 (2007)
21. R. Driben, I.M. Merhasin, B.V. Gisin, B.A. Malomed, Finite-band solitons in the kronig-penney model with the cubic-quintic nonlinearity. Phys. Rev. E **71**, 016613 (2005)
22. E.A. Ostrovskaya, Y.S. Kivshar, Photonic crystals for matter waves: Bose-einstein condensates in optical lattices. Opt. Exp. **12**, 19–29 (2004)
23. H. Sakaguchi, B.A. Malomed, Two-dimensional loosely and tightly bound solitons in optical lattices and inverted traps. J. Phys. B: At. Mol. Opt. Phys. **37**, 2225–2239 (2004)
24. F.W. Wise, Y.-F. Chen, K. Beckwitt, B.A. Malomed, Criteria for the experimental observation of multidimensional optical solitons in saturable media. Phys. Rev. E **70**, 046610 (2004)
25. Z. Shi, J. Yang, Solitary waves bifurcated from bloch-band edges in two-dimesional periodic media. Phys. Rev. E **75**, 056602 (2007)
26. B. Ilan, M.I. Weinstein, Band-edge solitons, nonlinear schrödinger / gross-pitaevskii equations and effective media. SIAM Multiscale Model. Simul. **8**, 1055–1101 (2010)
27. M.J. Ablowitz, B. Ilan, E. Schonbrun, R. Piestun, Solitons in two-dimensional lattices possessing defects, dislocations, and quasicrystal structures. Phys. Rev. E **74**, 035601(R) (2006)
28. B. Freedman, G. Bartal, M. Segev, R. Lifshitz, D.N. Christodoulides, J.W. Fleischer, Wave and defect dynamics in nonlinear photonic quasicrystals. Nature **440**, 1166–1169 (2006)
29. H. Sakaguchi, B.A. Malomed, Gap solitons in quasiperiodic optical lattices. Phys. Rev. E **74**, 026601 (2006)
30. P.R Wallace, The band theory of graphite. Phys. Rev. **71**, 622 (1947)
31. O. Bahat-Treidel, O. Peleg, M. Segev, Symmetry breaking in honeycomb photonic lattices. Opt. Lett. **33**, 2251–2253 (2008)
32. M.J. Ablowitz, Y. Zhu, Nonlinear diffraction in photonic graphene. Opt. Lett. **36**, 3762–3764 (2011)
33. F.D.M. Haldane, S. Raghu, Possible realization of directional optical waveguides in photonic crystals with broken time-reversal symmetry. Phys. Rev. Lett. **100**, 013904 (2008)
34. S. Raghu, F.D.M. Haldane, Analogs of quantum hall effect edge states in photonic crystals. Phys. Rev. A **78**, 033834 (2008)
35. M.J. Ablowitz, Y. Zhu, Nonlinear waves in shallow honeycomb lattices. SIAM J. Appl. Math. **72**, 240–260 (2012)
36. O. Bahat-Triedel, A. Szameit, M. Rechtsman, M. Segev, $\mathcal{PT}$-symmetry in honeycomb photonic lattices. Phys. Rev. A **84**, 021806(R) (2011)

37. H. Ramezani, T. Kottos, V. Kovanis, D.N. Christodoulides, Exceptional-point dynamics in photonic honeycomb lattices with $\mathcal{PT}$ symmetry. Phys. Rev. A **85**, 013818 (2012)
38. O. Bahat-Treidel, O. Peleg, M. Segev, H. Buljan, Breakdown of Dirac dynamics in honeycomb lattices due to nonlinear interactions. Phys. Rev. A **82**, 013830 (2010)
39. O. Bahat-Treidel, O. Peleg, M. Grobman, N. Shapira, M. Segev, T. Pereg-Barnea, Klein tunneling in deformed honeycomb lattices. Phys. Rev. Lett. **104**, 063901 (2010)
40. C.L. Fefferman, M. Weinstein, Honeycomb lattice potentials and Dirac points. J. Amer. Math. Soc. **25**, 1169–1220 (2012)
41. M.J. Ablowitz, *Nonlinear Dispersive Waves: Asymptotic Analysis and Solitons* (Cambridge University Press, New York, 2011)
42. N.W. Ashcroft, N.D. Mermin, *Solid State Physics* (Brooks Cole, Brooks, 1978)
43. M. Reed, B. Simon, *Methods of Mathematical Physics IV: Analysisi of operators* (Acdemic Press, New York, 1978)
44. J. Yang, *Nonlinear Waves in Integrable and Nonintegrable Systems* (Society for Industrial and Applied Mathematics, Philadelphia, 2010)
45. M.J. Ablowitz, C.W. Curtis, Y. Zhu, On tight binding approximations in optical lattices. Stud. Appl. Math. **129**, 366–388 (2012)
46. G.L. Alfimov, P.G. Kevrekidis, V.V. Konotop, M. Salerno, Wannier functions analysis of the nonlinear schröinger equation with a periodic potential. Phys. Rev. E, **66**, 046608 (2002)
47. M.J. Ablowitz, J. Villarroel, On the Kadomtsev-Petviashili equation and associated constrints. Stud. Appl. Math. **85**, 195–213 (1991)